

# The Spin–Spin Coupling Constants in Ethane, Methanol and Methylamine: A Comparison of DFT, MCSCF and CCSD Results

Magdalena Pecul<sup>1</sup>, and Trygve Helgaker<sup>2</sup>

<sup>1</sup> Department of Chemistry, University of Warsaw, Pasteura 1, 02-093 Warsaw, Poland.

E-mail: magda@maja.chem.uw.edu.pl

<sup>2</sup> Department of Chemistry, University of Oslo, Box 1033, Blindern, N-0315 Oslo, Norway

*Received: 12 September 2002 / Accepted: 10 December 2002 / Published: 25 February 2003*

---

**Abstract:** The spin–spin coupling constants in ethane, methylamine, and methanol have been calculated using density-functional theory (DFT), coupled-cluster singles-and-doubles (CCSD) theory, and multiconfigurational self-consistent field (MCSCF) theory so as to benchmark the performance of DFT against high-level *ab initio* methods and experimental data. For each molecule, the Karplus curve has been evaluated at the three computational levels. The comparisons with *ab initio* methods indicate that DFT reproduces the  $^1J(\text{CH})$ ,  $^1J(\text{CC})$ , and  $^1J(\text{NH})$  one-bond couplings well but is less accurate for  $^1J(\text{CN})$ ,  $^1J(\text{OH})$ , and  $^1J(\text{CO})$ . While DFT performs well for the geminal couplings  $^2J(\text{HH})$  and  $^2J(\text{CH})$ , it tends to overestimate the vicinal  $^3J(\text{HH})$  couplings slightly although it is sufficiently accurate for most purposes.

**Keywords:** Spin–spin coupling constants, density-functional theory, Karplus curve.

---

## 1 Introduction

The indirect nuclear spin–spin coupling constants are, along with the nuclear shielding constants, the most important parameters of NMR spectra. Progress in NMR techniques—in particular, the use of high magnetic fields—has made possible the accurate measurement of a wide variety of NMR coupling constants, even in proteins and nucleic acids (and their complexes) of substantial size. In particular, since the nuclear spin–spin coupling constants are extremely sensitive to the molecular geometry, they have for a long time been used for structure assignments of such systems [1–4]. Such advances in NMR measurement techniques call for a concomitant development of computational methods suitable for the modelling of spin–spin coupling constants in large molecules, allowing for a better understanding of the correlation between NMR parameters and molecular structure. Over the last decade, NMR shielding constants have been calculated routinely for a vast range of systems [5–7]. By contrast, *ab initio* calculations of spin–spin coupling constants in molecules containing more than 10–12 atoms have been carried out only recently [5, 8–10]. The reason for this difference lies in the failure of the simplest and least expensive *ab initio* method—the Hartree–Fock method—to provide spin–spin coupling constants with acceptable accuracy because of the instability or near-instability of this wave function to triplet perturbations as generated by the Fermi contact and spin–dipole operators [5]. Although the multiconfigurational self-consistent field (MCSCF) and coupled-cluster methods are well suited to the calculation of spin–spin coupling constants, they are computationally expensive, making them impractical for example for biochemical systems. The recent development of techniques for the calculation of spin–spin coupling constants by Kohn–Sham density-functional theory (DFT)—which does not suffer from triplet instabilities in principle and which, even when using some proportion of exact exchange, is not much more expensive than the Hartree–Fock method—has provided a highly promising tool for the study of spin–spin couplings of large systems [11–15]. However, some problems inherent in the DFT method should be addressed first. Unlike wave-function methods such as the MCSCF and coupled-cluster methods, DFT is not hierarchical. As a result, it is often difficult to predict the relative performance of the different functionals. Therefore, before DFT is applied to the calculation of unknown coupling constants, a careful comparison of the spin–spin coupling constants obtained for some simple molecules by DFT and by wave-function methods such as the coupled-cluster singles-and-doubles (CCSD) and MCSCF theories is required. Some work has been already done in this direction [14, 16]. Thus, it has been established that, while DFT in general performs quite well for spin–spin coupling constants, certain couplings—in particular, those involving fluorine—cannot be accurately predicted by DFT using the present functionals [12, 14]. In the current work, we extend these comparisons to  $\text{CH}_3\text{CH}_3$ ,  $\text{CH}_3\text{NH}_2$  and  $\text{CH}_3\text{OH}$ . The molecules investigated in this paper are rather simple, without multiple carbon–carbon bonds or carbonyl

groups. On the other hand, all the important coupling constants of organic chemistry are present in  $\text{CH}_3\text{CH}_3$ ,  $\text{CH}_3\text{NH}_2$  and  $\text{CH}_3\text{OH}$ , making these molecules particularly suitable for testing DFT against high-level wave-function methods. In addition, the molecules under study here offer the possibility of calculating the dependence of  $^3J(\text{HH})$  on the dihedral angle—that is, the Karplus curve [1, 2], an important relationship in structural chemistry [1–3].

## 2 Computational details

The DFT calculations of the spin–spin coupling constants have been carried out using the approach of Helgaker, Watson and Handy [14]. In particular, the sum-over-state contributions to the spin–spin coupling constants are obtained analytically, using the linear-response formalism [14]. Moreover, unlike the original implementations of Malkina, Salahub and Malkin [11, 12] and of Dickson and Ziegler [15], in which only the local-density approximation (LDA) and the generalized-gradient approximation (GGA) can be used, the implementation of Helgaker and coworkers allows for the use of the exact Hartree–Fock exchange. The latter is an important point since the use of hybrid functionals such as B3LYP improves considerably the calculated spin–spin coupling constants [14]. Accordingly, all DFT results presented here have been obtained with the Becke three-parameter Lee–Yang–Parr (B3LYP) functional [17, 18]. The DFT calculations of spin–spin coupling constants have been carried out using an experimental version of the DALTON program [19]. For details on the DFT implementation, see Ref. [14]. The calculations of the spin–spin coupling constants at the MCSCF level [5, 20] have been carried out by means of DALTON 1.2 [19]. The restricted active-space (RAS) approach has been employed, with the nonhydrogen  $1s$  orbitals in the inactive subspace and with the seven Hartree–Fock-occupied valence orbitals in the RAS2 subspace. While the RAS-0 wave function contains in the RAS3 subspace 20 orbitals (for  $\text{CH}_3\text{CH}_3$ ) or 19 orbitals (for  $\text{CH}_3\text{NH}_2$  and  $\text{CH}_3\text{OH}$ ), the RAS-I wave function contains 30 (for  $\text{CH}_3\text{CH}_3$ ) or 27 orbitals (for  $\text{CH}_3\text{NH}_2$  and  $\text{CH}_3\text{OH}$ ) in the RAS3 subspace. The RAS1 subspace is empty and a maximum of two electrons are allowed to be excited from RAS2 to RAS3. This construction of the MCSCF active space has previously been shown to provide good results for spin–spin coupling constants [21, 22]. Some of the MCSCF results have already been reported in Refs. [21, 22]. The CCSD spin–spin calculations have been carried out using linear-response theory—see Ref. [23] and references therein—as implemented in a program based on Aces II [24]. For a description of CCSD second derivatives in the unrestricted Hartree–Fock framework, see Ref. [25]. In the calculations presented here, all four terms—Fermi contact (FC), spin–dipole (SD), paramagnetic spin-orbit (PSO) and diamagnetic spin-orbit (DSO)—that contribute to nuclear spin–spin coupling constants in nonrelativistic theory have been calculated. The reported coupling constants have been averaged assuming free internal molecular rotation, except when the dependence on the

dihedral angle is discussed. The experimental equilibrium geometry [26–28] has been employed. The Karplus curves have been obtained changing only the dihedral angle, i.e. without taking into account geometry relaxation. It has been demonstrated before [22] that for the  $^3J(\text{HH})$  couplings in the molecule under study the results obtained with and without geometry relaxation are close to each other. The nitrogen coupling constants are given for isotope  $^{15}\text{N}$ . All calculations have been carried out in the IGLO-III basis [29]. Although not large, this basis should be sufficient for a qualitative prediction of spin–spin coupling constants, at least for the DFT calculations. However, for the MCSCF and in particular the CCSD calculations, in which dynamical correlation is described by means of virtual excitations, this basis is certainly not sufficiently large to recover the full effects of electron correlation. We therefore expect the CCSD calculations to be further away from the basis-set limit than are the DFT calculations. In addition, we have ignored the effect of triple excitations in the MCSCF and coupled-cluster calculations. Although we do not claim that the presented MCSCF and CCSD spin–spin couplings are close to the true nonrelativistic results, they are representative of the best spin–spin calculations that can nowadays be carried out for molecules of this size.

### 3 Results and discussion

Our discussion of the results is divided into three subsections, treating separately the one-bond, geminal and vicinal couplings. However, before examining the calculated and experimental constants in detail, we note that in no case do we expect a perfect agreement with experiment. First, the experimental spectra have been recorded for solvated molecules [30–32]. Although the solvent effects are probably small for the apolar solvents in these experiments, they are certainly not zero. Second, the IGLO-III [29] basis used here, although suitable for spin–spin coupling constants Refs. [5, 33], is far from complete. Third and perhaps most important, we have neglected the rovibrational contributions to the spin–spin coupling constants. Such contributions may be substantial for spin–spin coupling constants, which are sensitive to small changes in the geometry [21, 22, 34, 35].

#### 3.1 One-bond coupling constants

The total one-bond coupling constants calculated at the DFT, MCSCF and CCSD levels are compared with the experimental values in Table 1. The DFT  $^1J(\text{CH})$  coupling constants are in agreement with the MCSCF results but not with the CCSD ones. As previously observed [36], MCSCF and DFT give  $^1J(\text{CH})$  couplings closer to experiment than does CCSD. However, a better description of electron correlation in the MCSCF wave function reduces  $^1J(\text{CH})$  couplings [21, 22], shifting the values closer to the CCSD ones. The good agreement of the MCSCF and DFT values

Table 1: Comparison of the total one-bond coupling constants calculated at the DFT, RASSCF<sup>a</sup> and CCSD levels with experiment.<sup>b</sup>

		DFT	RASSCF	CCSD	exp.
CH <sub>3</sub> CH <sub>3</sub>	<sup>1</sup> J(CH)	122.6	120.3	114.1	125.19 – 125.238
CH <sub>3</sub> NH <sub>2</sub>	<sup>1</sup> J(CH)	129.5	128.3	120.9	132.2 (0.2)
CH <sub>3</sub> OH	<sup>1</sup> J(CH)	135.1	134.2	126.3	141
CH <sub>3</sub> NH <sub>2</sub>	<sup>1</sup> J(NH)	−63.3	−65.0	−61.7	−65.0 (0.2)
CH <sub>3</sub> OH	<sup>1</sup> J(OH)	−68.7	−78.5	−75.9	−85 (10)
CH <sub>3</sub> CH <sub>3</sub>	<sup>1</sup> J(CC)	32.6	38.4	34.1	34.498 – 34.558
CH <sub>3</sub> NH <sub>2</sub>	<sup>1</sup> J(CN)	−2.3	−6.5	−5.1	−4.5 (0.5)
CH <sub>3</sub> OH	<sup>1</sup> J(CO)	19.9	11.1	12.4	–

<sup>a</sup> The SD term obtained at the RAS-0 level, the remaining ones at the RAS-I level.

<sup>b</sup> Experimental results from Refs. [30–32] for CH<sub>3</sub>CH<sub>3</sub>, CH<sub>3</sub>NH<sub>2</sub> and CH<sub>3</sub>OH, respectively.

with experiment may therefore be coincidental. By the same argument, the difference between CCSD and experimental results may in part arise from rovibrational effects. For example, zero-point vibrational corrections have been found to increase <sup>1</sup>J(CH) in CH<sub>4</sub>, HCN, and HCCH [35] by approximately 5 Hz. This would bring CCSD values from Table 1 closer to the experimental numbers. The performance of DFT is poorer for the coupling constants of <sup>17</sup>O and <sup>15</sup>N. However, the DFT <sup>1</sup>J(NH) coupling in CH<sub>3</sub>NH<sub>2</sub> agrees much better with CCSD, MCSCF and experiment than does its counterpart <sup>1</sup>J(OH) in CH<sub>3</sub>OH. The latter coupling is close to the experimental value when calculated at the CCSD or MCSCF levels, whereas DFT underestimates the coupling. Also, a large discrepancy between the DFT and CCSD (and also MCSCF) results is observed for the <sup>1</sup>J(CO) and <sup>1</sup>J(CN) couplings in methanol and methylamine, respectively. In the case of <sup>1</sup>J(CN), the CCSD value is supported by experiment. These observations agree with the conclusions of Refs. [12, 14]—namely, that the performance of DFT deteriorates for couplings between nuclei with lone pairs. A better understanding of the performance of DFT method is gained by comparing the individual contributions to the one-bond coupling constants—see Table 2. As expected, the differences in the calculated <sup>1</sup>J(CH) couplings arise mostly from differences in the treatment of the FC contribution, which dominates the total couplings. For the SD, PSO, and DSO contributions, the MCSCF and CCSD values are close to each other. We further note that DFT gives <sup>1</sup>J(CN) and <sup>1</sup>J(CO) FC contributions in poor agreement with CCSD although, for <sup>1</sup>J(CN), also the MCSCF result disagrees with CCSD. For the SD contributions to the one-bond couplings, DFT performs surprisingly well—in many cases better (relative to CCSD) than does MCSCF. The discrepancies

Table 2: Comparison of individual contributions to the one-bond coupling constants calculated at the DFT, RASSCF<sup>a</sup> and CCSD levels.

	Fermi contact			Spin-dipole			Paramagnetic SO			Diamagnetic SO		
	DFT	RAS	CCSD	DFT	RAS	CCSD	DFT	RAS	CCSD	DFT	RAS	CCSD
CH <sub>3</sub> CH <sub>3</sub> <sup>1</sup> J(CH)	120.9	118.9	112.6	-0.1	-0.2	-0.2	1.3	1.2	1.2	0.5	0.5	0.5
CH <sub>3</sub> NH <sub>2</sub> <sup>1</sup> J(CH)	128.3	127.3	119.9	-0.1	-0.3	-0.2	0.8	0.7	0.7	0.5	0.5	0.6
CH <sub>3</sub> OH <sup>1</sup> J(CH)	134.2	133.6	125.5	-0.1	-0.3	-0.2	0.4	0.3	0.3	0.6	0.6	0.6
CH <sub>3</sub> NH <sub>2</sub> <sup>1</sup> J(NH)	-60.0	-62.1	-58.7	-0.2	-0.1	-0.1	-2.9	-2.7	-2.6	-0.2	-0.2	-0.2
CH <sub>3</sub> OH <sup>1</sup> J(OH)	-55.9	-66.9	-64.2	-0.6	-0.3	-0.5	-12.0	-11.2	-11.0	-0.2	-0.2	-0.3
CH <sub>3</sub> CH <sub>3</sub> <sup>1</sup> J(CC)	31.3	37.1	32.7	1.1	1.0	1.0	0.0	0.1	0.2	0.1	0.1	0.1
CH <sub>3</sub> NH <sub>2</sub> <sup>1</sup> J(CN)	-1.2	-5.2	-3.9	-0.8	-0.7	-0.7	-0.3	-0.5	-0.5	-0.1	-0.1	-0.1
CH <sub>3</sub> OH <sup>1</sup> J(CO)	23.5	14.7	16.1	-1.9	-1.7	-1.7	-1.7	-1.9	-2.0	-0.1	-0.1	-0.1

<sup>a</sup> The SD term obtained at the RAS-0 level, the remaining ones at the RAS-I level.

between DFT and the wave-function methods are larger for the PSO contributions. Predictably, the DSO contribution depends little on the computational level. In short, DFT performs very well for <sup>1</sup>J(CH), <sup>1</sup>J(CC) and <sup>1</sup>J(NH)—perhaps the most important one-bond coupling constants in chemistry. On the other hand, the DFT results should be treated with caution in the case of the one-bond oxygen couplings and the <sup>1</sup>J(CN) couplings.

### 3.2 Geminal coupling constants

The DFT, MCSCF, and CCSD results for the geminal (i.e, two-bond) coupling constants in CH<sub>3</sub>CH<sub>3</sub>, CH<sub>3</sub>NH<sub>2</sub> and CH<sub>3</sub>OH are compared with experiment in Table 3, while Table 4 contains the calculated individual contributions to the couplings. In comparing with experiment, we note that the geminal proton–proton couplings have been measured as proton–deuteron couplings for partially deuterated compounds and then rescaled with the appropriate gyromagnetic ratios, neglecting vibrational isotope effects. These effects are ignored in our calculations since we neglect vibrational corrections altogether. For CH<sub>3</sub>CH<sub>3</sub>, CH<sub>3</sub>NH<sub>2</sub> and CH<sub>3</sub>OH, all geminal spin–spin couplings are negative. We also note that, in magnitude, the coupled-cluster <sup>2</sup>J(CH) and <sup>2</sup>J(HH) couplings are bracketed by the smaller DFT couplings and by the larger RASSCF couplings. Concerning DFT, it performs in general very well for the <sup>2</sup>J(HH) coupling constants. In particular, its performance appears to be better than that of MCSCF, where large active spaces are needed to bring the calculated geminal coupling constants, especially <sup>2</sup>J(HH), into agreement with experiment [21, 22]. For the <sup>2</sup>J(CH) couplings, the discrepancies between DFT and CCSD

Table 3: Comparison of the total geminal coupling constants calculated at the DFT, RASSCF<sup>a</sup> and CCSD levels with experiment.<sup>b</sup>

		DFT	RASSCF	CCSD	exp.
CH <sub>3</sub> CH <sub>3</sub>	<sup>2</sup> J(CH)	-3.0	-5.5	-4.4	-4.655 – -4.661
CH <sub>3</sub> NH <sub>2</sub>	<sup>2</sup> J(CH)	-1.9	-4.4	-3.3	–
CH <sub>3</sub> OH	<sup>2</sup> J(CH)	-2.4	-4.2	-3.4	–
CH <sub>3</sub> CH <sub>3</sub>	<sup>2</sup> J(HH)	-11.3	-14.4	-12.1	–
CH <sub>3</sub> NH <sub>2</sub>	<sup>2</sup> J(HH) <sup>c</sup>	-10.1	-13.3	-11.1	–
CH <sub>3</sub> NH <sub>2</sub>	<sup>2</sup> J(HH) <sup>d</sup>	-7.6	-10.8	-9.3	–
CH <sub>3</sub> OH	<sup>2</sup> J(HH)	-9.2	-12.4	-10.2	-10.8
CH <sub>3</sub> NH <sub>2</sub>	<sup>2</sup> J(NH)	-3.0	-0.7	-0.9	-1.0 (0.1)
CH <sub>3</sub> OH	<sup>2</sup> J(OH)	-6.2	-5.0	-4.9	-7.5

<sup>a</sup> RASSCF results for the SD term obtained at the RAS-0 level, for the remaining ones at the RAS-I level.

<sup>b</sup> Experimental results from Refs. [30–32] for CH<sub>3</sub>CH<sub>3</sub>, CH<sub>3</sub>NH<sub>2</sub> and CH<sub>3</sub>OH, respectively.

<sup>c</sup> H–C–H coupling.

<sup>d</sup> H–N–H coupling.

are somewhat larger. Surprisingly, <sup>2</sup>J(OH) calculated at the DFT level is in better agreement with experiment than are the CCSD and MCSCF results, in spite of the usual poor performance of DFT for couplings to lone-pair atoms. However, in this case, the rather old experimental value may not be reliable, considering the difficulties associated with the measurement of couplings of highly quadrupolar nuclei such as <sup>17</sup>O. Indeed, the experimental value of <sup>2</sup>J(NH) in CH<sub>3</sub>NH<sub>2</sub> is much better reproduced by CCSD and MCSCF than by DFT, confirming this hypothesis. The individual contributions to the geminal coupling constants in Table 4 follow the same trends as for the one-bond coupling constants. Again, in all cases where a discrepancy between DFT and CCSD occurs, it is caused by the difficulties experienced by DFT in reproducing the dominant FC term—see, in particular, the contributions to <sup>2</sup>J(OH) and <sup>2</sup>J(NH). It is also interesting to note that, for the remaining (much smaller) contributions to the couplings, DFT performs much better than it does for FC. In particular, the DFT SD terms are consistent with the CCSD results, the differences being smaller than between CCSD and MCSCF. Furthermore, the DFT PSO contributions to the geminal couplings are in acceptable agreement with the CCSD results, although in this case MCSCF performs better. The calculated DSO terms are fairly independent on the level of the calculations.

Table 4: Comparison of individual contributions to the geminal coupling constants calculated at the DFT, RASSCF<sup>a</sup> and CCSD levels.

	Fermi contact			Spin-dipole			Paramagnetic SO			Diamagnetic SO		
	DFT	RAS	CCSD	DFT	RAS	CCSD	DFT	RAS	CCSD	DFT	RAS	CCSD
CH <sub>3</sub> CH <sub>3</sub> <sup>2</sup> J(CH)	-3.1	-5.6	-4.5	0.1	0.1	0.1	0.4	0.4	0.4	-0.3	-0.3	-0.3
CH <sub>3</sub> NH <sub>2</sub> <sup>2</sup> J(CH)	-2.1	-4.6	-3.5	0.1	0.1	0.1	0.7	0.7	0.7	-0.6	-0.6	-0.6
CH <sub>3</sub> OH <sup>2</sup> J(CH)	-2.6	-4.5	-3.6	0.0	0.1	0.0	0.9	0.9	0.9	-0.7	-0.7	-0.7
CH <sub>3</sub> CH <sub>3</sub> <sup>2</sup> J(HH)	-11.9	-15.0	-12.6	0.4	0.4	0.4	3.0	3.0	3.0	-2.9	-2.9	-2.9
CH <sub>3</sub> NH <sub>2</sub> <sup>2</sup> J(HH)	-10.6	-13.8	-11.5	0.4	0.5	0.4	2.9	2.8	2.8	-2.8	-2.8	-2.8
CH <sub>3</sub> NH <sub>2</sub> <sup>2</sup> J(HH) <sup>c</sup>	-9.1	-12.2	-10.6	0.6	0.7	0.6	5.6	5.4	5.4	-4.8	-4.8	-4.8
CH <sub>3</sub> OH <sup>2</sup> J(HH)	-9.7	-12.9	-10.6	0.5	0.5	0.5	2.9	2.8	2.8	-2.9	-2.9	-2.8
CH <sub>3</sub> NH <sub>2</sub> <sup>2</sup> J(NH)	-2.8	-0.6	-0.8	0.0	0.0	0.0	-0.3	-0.3	-0.3	0.1	0.2	0.2
CH <sub>3</sub> OH <sup>2</sup> J(OH)	-5.6	-4.5	-4.3	0.1	0.2	0.1	-1.0	-0.9	-0.9	0.2	0.2	0.2

<sup>a</sup> The SD term obtained at the RAS-0 level, the remaining ones at the RAS-I level.

<sup>b</sup> H–C–H coupling.

<sup>c</sup> H–N–H coupling.

### 3.3 Vicinal coupling constants

The averaged total vicinal proton–proton coupling constants and their individual contributions are presented in Tables 5 and 6, respectively. Comparing the values in Table 5, we observe the same behaviour as for the <sup>1</sup>J(CH) coupling constants. Thus, CCSD underestimates the experimental couplings, whereas the DFT couplings are quite close to experiment (except for <sup>3</sup>J(HH) in CH<sub>3</sub>OH). Also, the MCSCF results are bracketed by DFT and CCSD results. Bearing in mind the good CCSD performance for the other coupling constants (and for <sup>3</sup>J(HH) in CH<sub>3</sub>OH), it is tempting to attribute this particular discrepancy to rovibrational effects rather than to the failure of CCSD. Still, because of the rather small number of correlating orbitals in the basis set and the neglect of triples in the coupled-cluster calculations, we should be very careful in treating the CCSD results as benchmarks for MCSCF and DFT. The vicinal FC terms calculated at the DFT level are substantially larger than the CCSD results but close to the MCSCF values. None of the remaining contributions to the <sup>3</sup>J(HH) couplings vary significantly with the computational level. The calculated dependence of the vicinal coupling constant <sup>3</sup>J(HH) on the dihedral angle is illustrated in Figs. 1, 2, and 3 for ethane, methylamine, and methanol, respectively. The MCSCF values have been obtained at the RAS-0 level. For comparison, the figures also contain empirical curves [3]. For CH<sub>3</sub>NH<sub>2</sub> and CH<sub>3</sub>OH, the empirical curves have been obtained from a set of

Table 5: Comparison of the total vicinal coupling constants calculated at the DFT, RASSCF<sup>a</sup> and CCSD levels with experiment.<sup>b</sup>

		DFT	RASSCF	CCSD	exp.
CH <sub>3</sub> CH <sub>3</sub>	<sup>3</sup> J(HH)	7.8	7.3	6.7	7.992 – 8.005
CH <sub>3</sub> NH <sub>2</sub>	<sup>3</sup> J(HH)	6.9	6.3	5.8	7.1 (0.1)
CH <sub>3</sub> OH	<sup>3</sup> J(HH)	5.9	5.1	4.8	5.0

<sup>a</sup> The SD term obtained at the RAS-0 level, the remaining ones at the RAS-I level.

<sup>b</sup> Experimental results from Refs. [30–32] for CH<sub>3</sub>CH<sub>3</sub>, CH<sub>3</sub>NH<sub>2</sub> and CH<sub>3</sub>OH, respectively.

Table 6: Comparison of individual contributions to the vicinal coupling constants calculated at the DFT, RASSCF<sup>a</sup> and CCSD levels.

	Fermi contact			Spin-dipole			Paramagnetic SO			Diamagnetic SO		
	DFT	RAS	CCSD	DFT	RAS	CCSD	DFT	RAS	CCSD	DFT	RAS	CCSD
CH <sub>3</sub> CH <sub>3</sub> <sup>3</sup> J(HH)	7.8	7.3	6.7	0.1	0.1	0.1	1.6	1.6	1.5	−1.6	−1.6	−1.6
CH <sub>3</sub> NH <sub>2</sub> <sup>3</sup> J(HH)	6.9	6.4	5.9	0.0	0.1	0.1	2.1	2.0	2.0	−2.1	−2.1	−2.1
CH <sub>3</sub> OH <sup>3</sup> J(HH)	5.9	5.1	4.9	0.1	0.1	0.1	2.5	2.4	2.4	−2.5	−2.5	−2.5

<sup>a</sup> The SD term obtained at the RAS-0 level, the remaining ones at the RAS-I level.

compounds containing the –CH<sub>2</sub>OH and –CHNH<sub>2</sub> groups, respectively; for CH<sub>3</sub>CH<sub>3</sub>, they have been generated from couplings in substituted cyclohexanones (curve labeled exp<sup>\*</sup>) and in ethane derivatives (curve labeled exp<sup>\*\*</sup>). As for the torsionally averaged <sup>3</sup>J(HH) couplings, the DFT <sup>3</sup>J(HH) constants are, for all dihedral angles, larger than those obtained by CCSD; the MCSCF values usually fall between. However, unlike for the averaged <sup>3</sup>J(HH) couplings, the larger DFT values are in poorer agreement with experiment, especially for angles close to 0° or 180°. Clearly, a comparison with empirical curves determined for different compounds has only a limited value. The overestimation of DFT relative to CCSD is approximately constant for all angles, varying from 15% for CH<sub>3</sub>CH<sub>3</sub> to 20% for CH<sub>3</sub>OH. An interesting point is that <sup>3</sup>J(HH) transmitted through H–C–O–H bonds seems to become negative when the dihedral angle approaches 90°, at all computational levels. It would be worthwhile to verify this experimentally, although appropriate model compounds would be difficult to find.

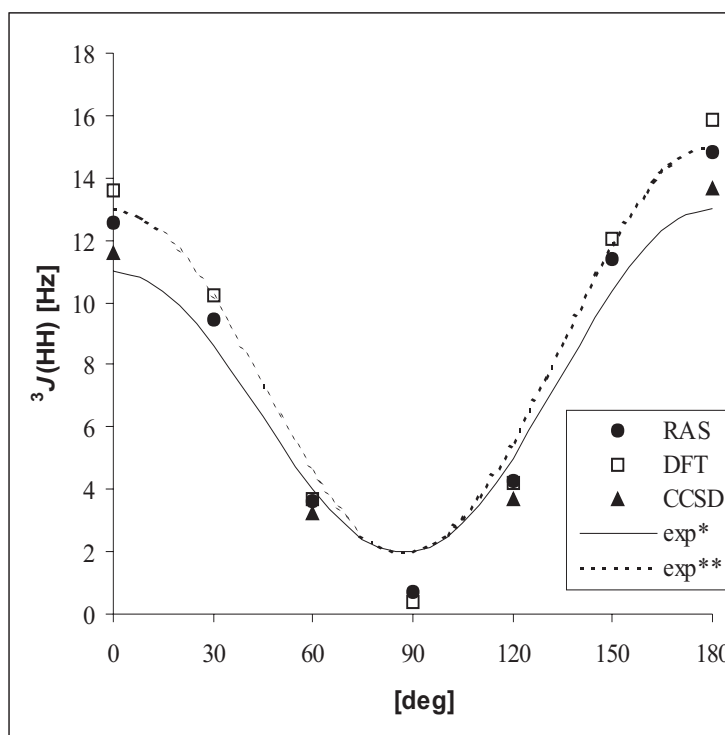


Figure 1: Comparison of the Karplus curve for ethane calculated at the DFT level, the MCSCF level (RAS-0 results from Ref. [21]) and the CCSD level with an empirical curve [3].

#### 4 Summary and conclusions

The performance of DFT for the calculation of spin–spin coupling constants has been examined on the basis of the couplings in  $\text{CH}_3\text{CH}_3$ ,  $\text{CH}_3\text{NH}_2$ , and  $\text{CH}_3\text{OH}$ . In particular, B3LYP results have been compared with experimental results and with high-level MCSCF and CCSD wave-function calculations. It is rewarding that DFT gives the important one-bond coupling constants of carbon such as  $^1J(\text{CH})$  and  $^1J(\text{CC})$  close to experiment, although it is possible that, in a few cases, the good agreement arises from error cancellation. DFT works well also for the important class of  $^1J(\text{NH})$  one-bond coupling constants, but notably not for  $^1J(\text{OH})$ . The  $^1J(\text{CN})$  couplings should also be viewed with caution, considering the relatively large difference between DFT and CCSD in  $\text{CH}_3\text{NH}_2$ . Although the  $^1J(\text{CO})$  coupling in  $\text{CH}_3\text{OH}$  is apparently also inaccurately calculated by DFT, this is less important since, unlike  $^1J(\text{CN})$ , this coupling is unlikely to be used as a structural parameter. DFT performs satisfactorily for the geminal proton–proton couplings, which are very challenging for the MCSCF method. The agreement with CCSD is slightly worse for  $^2J(\text{CH})$  and deteriorates substantially for  $^2J(\text{NH})$  and  $^2J(\text{OH})$ . In the case of the vicinal proton–proton

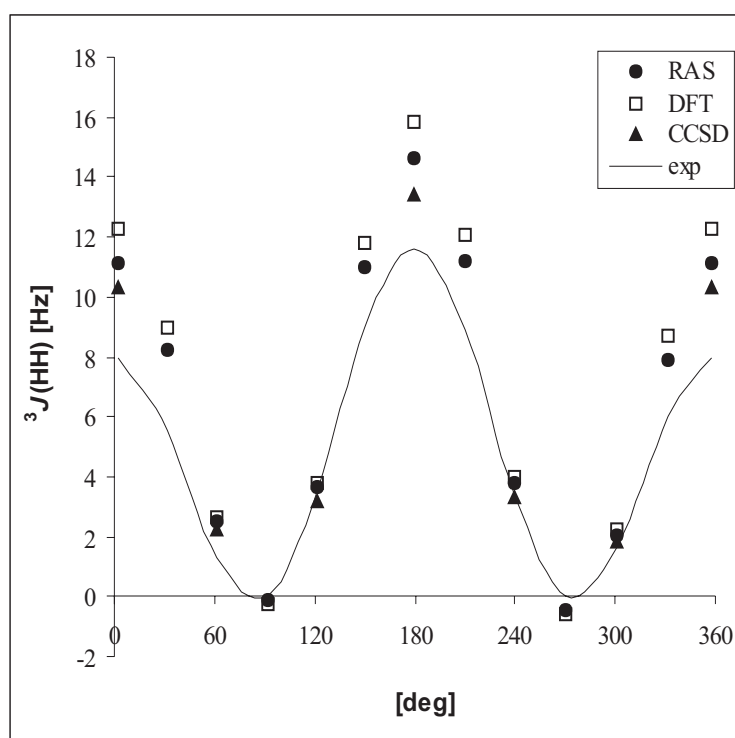


Figure 2: Comparison of the Karplus curve for methylamine obtained at the DFT level the MCSCF level (RAS-0 results from Ref. [22]) and the CCSD level with an empirical curve [3].

coupling constants—the most important couplings in structural investigations—DFT is reliable, although the total values tend to be overestimated in comparison with MCSCF and CCSD (and, in one case, with experiment). The analysis of the dependence of  ${}^3J(\text{HH})$  on the dihedral angle show that the overestimation of the CCSD values by DFT is approximately 15–20% for all three molecules. Obviously, it should be taken into account that the comparison with experiment is limited. First, the employed basis set is relatively small. Second and more important, the vibrational corrections, which for spin–spin coupling constants may be substantial, have not been taken into account. Finally, solvent effects have been neglected. We therefore believe that, in this case, it is more useful to compare DFT with CCSD and MCSCF than with experiment, but note that our coupled-cluster calculations suffer from a small basis and the neglect of triples. In all cases where a discrepancy occurs between the DFT spin–spin coupling and the CCSD and MCSCF couplings, it can be traced to the FC term. However, this occurs mainly because of the dominance of this term in the couplings under study. In many cases, a large difference between DFT and CCSD (and MCSCF) results is observed for the PSO term. The small SD terms are rendered adequately by DFT, as are the DSO terms.

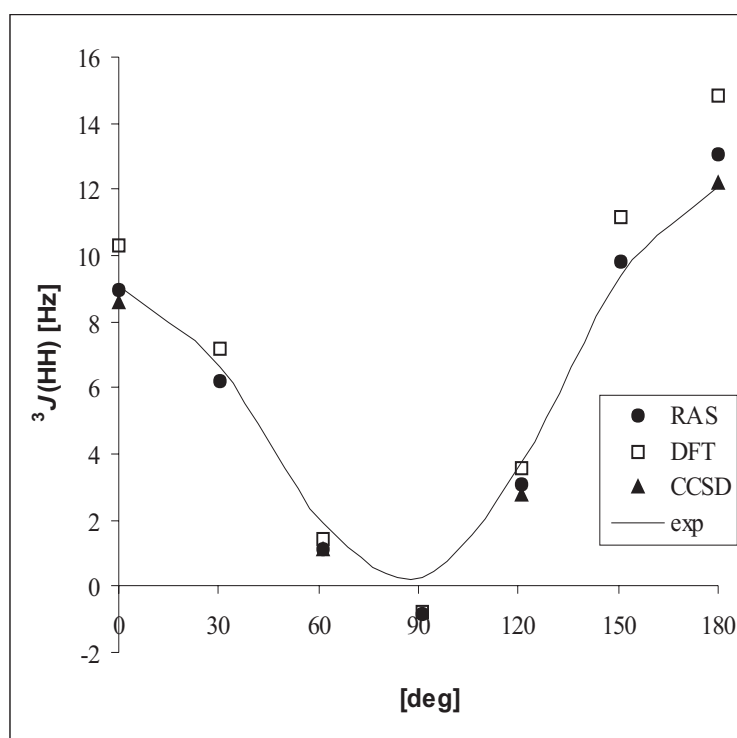


Figure 3: Comparison of the Karplus curve for methanol obtained at the DFT level the MCSCF level (RAS-0 results from Ref. [22]) and the CCSD level with an empirical curve [3].

## Acknowledgments

We are grateful to O. Christiansen, J. Gauss, and J. Stanton for allowing us to use their development version of the ACES II code. This work has been supported by the 7 TO9A 11121 KBN Grant and the European Research and Training Network: “Molecular Properties and Molecular Materials” (MOLPROP), Contract No. HPRN-CT-2000-00013.

## References

- [1] Karplus, M. Contact Electron-Spin Coupling of Nuclear Magnetic Moments. *J. Chem. Phys.* **1959**, *30*, 11–15.
- [2] Karplus, M. Vicinal Proton Coupling in NMR. *J. Am. Chem. Soc.* **1963**, *85*, 2870–2871.
- [3] Minch, M. J. Orientational Dependence of Vicinal Proton-Proton NMR Coupling Constants: The Karplus Relationship. *Conc. Magn. Reson.* **1994**, *6*, 41–56.

- [4] Juranic, N.; Ilich, P. K.; and Macura, S. Hydrogen Bonding Networks in Proteins As Revealed by the Amide  $^1J_{NC'}$  Coupling Constant. *J. Am. Chem. Soc.* **1995**, *117*, 405–410.
- [5] Helgaker, T.; Jaszunski, M.; and Ruud, K. Ab initio methods for the calculation of NMR shielding and indirect spin-spin coupling constants. *Chem. Rev.* **1999**, *99*, 293–352.
- [6] de Dios, A. C. Ab initio calculations of the NMR chemical shift. *Prog. NMR. Spectrosc.* **1996**, *29*, 229–278.
- [7] Fukui, H. Theory and calculation of nuclear shielding constants. *Prog. NMR. Spectrosc.* **1997**, *31*, 317–342.
- [8] Pecul, M.; Leszczynski, J.; and Sadlej, J. The shielding constants and scalar couplings in N-H...O=C and N- H...N=C hydrogen bonded systems: an *ab initio* MO study. *J. Phys. Chem. A* **2000**, *104*, 8105–8113.
- [9] Scheurer, C.; and Brüschweiler, R. Quantum-Chemical Characterization of Nuclear Spin-Spin Couplings Across Hydrogen Bonds. *J. Am. Chem. Soc.* **1999**, *121*, 8661–8662.
- [10] Peralta, J. E.; Barone, V.; and Contreras, R. H. Through-Bond and Through-Space  $J_{FF}$  Spin-Spin Couplings in Perifluoronaphtalenes: Accurate DFT Evaluation of the Four Contribution. *J. Am. Chem. Soc.* **2001**, *123*, 9162–9163.
- [11] Malkin, V. G.; Malkina, O. L.; and Salahub, D. R. Calculation of spin-spin coupling constants using density functional theory. *Chem. Phys. Lett.* **1994**, *221*, 91–99.
- [12] Malkina, O. L.; Salahub, D. R.; and Malkin, V. G. Nuclear magnetic resonance spin-spin coupling constants from density functional theory: Problems and results. *J. Chem. Phys.* **1996**, *105*, 8793–8800.
- [13] Sychrovský, V.; Gräfenstein, J.; and Cremer, D. Nuclear magnetic resonance spin–spin coupling constants from coupled perturbed density functional theory. *J. Chem. Phys.* **2000**, *113*, 3530–3547.
- [14] Helgaker, T.; Watson, M.; and Handy, N. C. Analytical calculation of nuclear magnetic resonance spin-spin coupling constants at the generalized gradient approximation and hybrid levels of density functional theory. *J. Chem. Phys.* **2000**, *113*, 9402–9409.
- [15] Dickinson, R. M.; and Ziegler, T. NMR Spin-Spin Coupling Constants from Density Functional Theory with Slater-Type Basis Functions. *J. Phys. Chem.* **1996**, *100*, 5286–5290.

- [16] Lantto, P.; Vaara, J.; and Helgaker, T. Spin–spin coupling tensors by density-functional linear response theory. *J. Chem. Phys.* **2002**, *117*, 5998–6009.
- [17] Becke, A. D. Density-functional thermochemistry. III. The role of exact exchange. *J. Chem. Phys.* **1993**, *98*, 5648–5652.
- [18] Stephens, P. J.; Devlin, F. J.; Chabalowski, C. F.; and Frisch, M. J. Ab Initio Calculation of Vibrational Absorption and Circular Dichroism Spectra Using Density Functional Force Fields. *J. Phys. Chem.* **1994**, *98*, 11623–11627.
- [19] Helgaker, T.; Jensen, H. J. A.; Jørgensen, P.; Olsen, J.; Ruud, K.; Ågren, H.; Auer, A. A.; Bak, K. L.; Bakken, V.; Christiansen, O.; Coriani, S.; Dahle, P.; Dalskov, E. K.; Enevoldsen, T.; Fernandez, B.; Hättig, C.; Hald, K.; Halkier, A.; Heiberg, H.; Hettema, H.; Jonsson, D.; Kirpekar, S.; Kobayashi, R.; Koch, H.; Mikkelsen, K. V.; Norman, P.; Packer, M. J.; Pedersen, T. B.; Ruden, T. A.; Sanchez, A.; Saue, T.; Sauer, S. P. A.; Schimmelpfenning, B.; Sylvester-Hvid, K. O.; Taylor, P. R.; and Vahtras, O. DALTON, an *ab initio* electronic structure program, Release 1.2 (2001). See <http://www.kjemi.uio.no/software/dalton/dalton.html>.
- [20] Vahtras, O.; Ågren, H.; Jørgensen, P.; Jensen, H. J. A.; Padkjær, S. B.; and Helgaker, T. Indirect nuclear spin-spin coupling constants from multiconfigurational linear response theory. *J. Chem. Phys.* **1992**, *96*, 6120–6125.
- [21] Pecul, M.; Jaszuński, M.; and Sadlej, J. The geometry dependence of the spin-spin coupling constants in ethane: a theoretical study. *Chem. Phys. Lett.* **1999**, *305*, 139–145.
- [22] Pecul, M.; and Sadlej, J. The nuclear spin-spin coupling constants in methanol and methylamine: geometry and solvent effects. *Chem. Phys.* **2000**, *255*, 137–148.
- [23] Auer, A. A.; and Gauss, J. Triple excitation effects in coupled-cluster calculations of indirect spin-spin coupling constants. *J. Chem. Phys.* **2001**, *115*, 1619–1622.
- [24] Stanton, J. F.; Gauss, J.; Watts, J. D.; Lauderdale, W. J.; and Bartlett, R. J. The Aces II Program System. *Int. J. Quantum Chem.:Quantum Chem. Symp.* **1992**, *26*, 879–894.
- [25] Szalay, P. G.; Gauss, J.; and Stanton, J. Analytic UHF-CCSD(T) second derivatives. *Theor. Chem. Acc.* **1998**, *100*, 5–11.
- [26] Hirota, E.; Endo, Y.; and Saito, S. Microwave Spectra of Deuterated Ethanes: Internal Rotation Potential Function and  $r_z$  Structure. *J. Mol. Spectrosc.* **1981**, *89*, 285–295.

- [27] Takagi, K.; and Kojima, T. Microwave spectrum of methylamine. *J. Phys. Soc. Japan.* **1971**, *30*, 1145–1157.
- [28] Gerry, M. C. L.; Lees, R. M.; and Winnewisser, G. The torsion-rotation microwave spectrum of  $^{12}\text{CH}_3^{18}\text{OH}$  and the structure of methanol. *J. Mol. Spectrosc.* **1976**, *61*, 231–242.
- [29] Schindler, M.; and Kutzelnigg, W. Theory of magnetic susceptibilities and NMR chemical shifts in terms of localized quantities. II. Application to some simple molecules. *J. Chem. Phys.* **1982**, *76*, 1919–1933.
- [30] Kaski, J.; Lantto, P.; Vaara, J.; and Jokisaari, J. Experimental and Theoretical ab initio Study of the  $^{13}\text{C}$ - $^{13}\text{C}$  Spin-Spin Coupling and  $^1\text{H}$  and  $^{13}\text{C}$  Shielding Tensors in Ethane, Ethene and Ethyne. *J. Am. Chem. Soc.* **1998**, *120*, 3993–4005.
- [31] Lazzeretti, P. Calculation of nuclear spin-spin coupling constants in methanol molecule. *J. Chem. Phys.* **1979**, *71*, 2614–2521.
- [32] Paolillo, L.; and Becker, E. D. The Relative Signs of the Spin-Spin Coupling Constants in  $\text{CH}_3\text{NH}_2$ . *J. Magn. Reson.* **1970**, *3*, 200–203.
- [33] Helgaker, T.; Jaszuński, M.; Ruud, K.; and Górska, A. Basis set dependence of nuclear spin-spin coupling constants. *Theor. Chim. Acc.* **1998**, *99*, 175–182.
- [34] Kirpekar, S.; Enevoldsen, T.; Oddershede, J.; and Raynes, W. T. Vibrational and thermal averaging of the indirect nuclear spin-spin coupling constants of  $\text{CH}_4$ ,  $\text{SiH}_4$ ,  $\text{GeH}_4$ , and  $\text{SnH}_4$ . *Mol. Phys.* **1997**, *91*, 897–907.
- [35] Ruden, T. A. ; Lutnæs, O. B. ; Helgaker, T.; and Ruud, K. Vibrational corrections to indirect nuclear spin-spin coupling constants calculated by density-functional theory. *J. Chem. Phys.*, submitted.
- [36] Pecul, M.; Dodziuk, H.; Jaszuński, M.; Lukin, O.; and Leszczynski, J. Ab initio calculations of the NMR spectra of [1,1,]propellane and bicyclo[1,1,1]pentane. *Phys. Chem. Chem. Phys.* **2001**, *3*, 1986–1991.